Arabian Journal of Chemistry (2022) 15, 103523

King Saud University

Arabian Journal of Chemistry

www.ksu.edu.sa
www.sciencedirect.com

ORIGINAL ARTICLE

Copper nanoparticles supported on polyethylene glycol-modified magnetic Fe_3O_4 nanoparticles: Its anti-human gastric cancer investigation

Zhisheng Liu [a,1], **Kai Wang** [a,1], **Tingting Wang** [a], **Ye Wang** [a], **Yunjie Ge** [b,*]

[a] *Department of General Surgery, Affiliated Qingdao Hiser Hospital of Qingdao University (Qingdao Hospital of Traditional Chinese Medicine), Qingdao, Shandong 266033, China*
[b] *Department of Healthcare Internal Medicine, Affiliated Qingdao Municipal Hospital of Qingdao University, Qingdao, Shandong 266000, China*

Received 28 July 2021; accepted 24 October 2021
Available online 29 October 2021

KEYWORDS

PEG;
Cu nanoparticles;
Nonmagnetic;
Human gastric cancer;
Antioxidant

Abstract In that work, we have described the synthesis of novel Cu NPs decorated polyethylene glycol (PEG_{2000}) coated magnetic nanoparticles (Fe_3O_4/PEG2000/Cu NPs) in an eco-friendly pathway applying *Green Tea* extract as reducing/stabilizing agent. The morphological and physicochemical features of the prepared nanocomposite were determined using several advanced techniques like ICP-OES, FE-SEM, EDX, atomic mapping, TEM, VSM, and XRD studies. In the antioxidant test, the IC50 of Fe_3O_4/PEG_{2000}/Cu nanocomposite and BHT against DPPH free radicals were 198 and 85 µg/mL, respectively. In the cellular and molecular part of the recent study, the treated cells with Fe_3O_4/PEG_{2000}/Cu nanocomposite were assessed by MTT assay for 48 h about the cytotoxicity and anti-human gastric cancer properties on normal (HUVEC) and gastric cancer cell lines i.e. NCI-N87 and MKN45. The IC50 of Fe_3O_4/PEG_{2000}/Cu nanocomposite were 316 and 131 µg/mL against NCI-N87 and MKN45 cell lines, respectively. The viability of malignant gastric cell line reduced dose-dependently in the presence of Fe_3O_4/PEG_{2000}/Cu nanocomposite. It seems that the anti-human gastric cancer effect of recent nanoparticles is due to their antioxidant effects.

1. Introduction

One of the simplest nanostructures that is widely used in industry today is metallic nanoparticles. Metallic nanoparticles can bind non-destructively to single-stranded DNA, which are important in medical diagnostics. Nanoparticles also can pass through the vessel and position the target organ in the body, which is used in biomedicine, imaging and therapy (Arunachalam et al., 2003; You et al., 2012; Mao et al.,

* Corresponding author.
E-mail address: qdgeyj@sina.com (Y. Ge).
[1] These authors are contributed equally to the article.
Peer review under responsibility of King Saud University.

ELSEVIER Production and hosting by Elsevier

https://doi.org/10.1016/j.arabjc.2021.103523
1878-5352

2016; LaVan et al., 2003). Biomedical applications of nanoparticles include drug carriers, tracking or labeling materials, carriers for gene therapy, hyperthermia, and materials for magnetic resonance imaging. To use nanoparticles to deliver a drug molecule or DNA or a gene in gene therapy, chemical changes at the nanoparticle surface are always required for specific interactions with the desired biomolecule. Nanoparticles are used for imaging for medical purposes or *in vitro* and *in vivo* chemical processes. Metallic nanoparticles have received a lot of attention due to their properties such as antifungal, photocatalytic and UV absorbing properties (Shi et al., 2011; Langer, 1990; Staroverov et al., 2009). Due to the antibacterial properties of these metal oxide nanoparticles, they can be used in the food industry and active food packaging. Also, metallic nanoparticles are potentially used in hyperthermia, magnetic resonance imaging (MRI), diagnosis and treatment of tumors or cancer, biomarkers, biodegradation, biotechnology and the removal of important organic, inorganic and radioactive contaminants due to their high biocompatibility (Shi et al., 2011; Langer, 1990; Staroverov et al., 2009; Bastus et al., 2009). Metallic nanoparticles have many applications in various fields such as fuel cells (hydrogen, methanol), glucose detection, drug delivery, toxicology, and biological interactions (Staroverov et al., 2009; Bastus et al., 2009). Metallic nanoparticles as a strong antioxidant resource are much less toxic than metals and also these nanoparticles have high power in scavenging free radicals (FR), so, it can be used as a natural antioxidant. Studies show that these nanoparticles detoxify hydroperoxidases and lipohydroperoxidases at the cytoplasmic and mitochondrial matrix levels. Metallic nanoparticles such as copper, silver and titanium have very high antimicrobial properties that can be used in various industrial and biomedical sectors (Langer, 1990; Staroverov et al., 2009; Bastus et al., 2009; Bao et al., 2013). Nanoparticles can also be used as coatings on molecules to bind or interact with biological targets, to ensure the presence of these nanoparticles in the target part of the body, carriers are used to accurately deliver these nanoparticles, in which peptides have been introduced as one of the best carriers (Shi et al., 2011; Langer, 1990; Staroverov et al., 2009; Bastus et al., 2009). The as-developed materials have a wide spectrum of implications such as degradation of dyes and environmental contaminants, removal of heavy and toxic metals, development of bio-engineering protocols, drug delivery, optometry, sensing, catalysis and biomedical science (Celardo et al., 2011).

The last decade has seen the promising emergence of nanoparticles in cancer treatment systems such as drug delivery and recombinant proteins with anti-tumor properties. Special features of the microenvironment around the tumor allow nanoscale systems to accumulate at the tumor site (De Jong and Borm, 2008; Borm et al., 2006; Stapleton and Nurkiewicz, 2014; Patra et al., 2018). Therefore, some nanoparticles with adjuvant properties, when they carry peptides or proteins, can increase the activity of cells in the reticuloendocardial system and activate macrophages and dendritic cells (Borm et al., 2006; Stapleton and Nurkiewicz, 2014; Patra et al., 2018; Itani and Al Faraj, 2019). Activated macrophages and dendritic cells swallow and process the complex, and immune responses are formed more efficiently. These nanoparticles can increase the response of the immune system to the target antigen, as well as to direct and direct this system to create a specific type of response (Trojer et al., 2013; Liu et al., 2014). By using these nanoparticles as antigen carriers, the amount of recombinant protein used as well as antigen toxicity is reduced and the destructive effects of proteases on protein antigen are reduced (Celardo et al., 2011; De Jong and Borm, 2008; Borm et al., 2006; Stapleton and Nurkiewicz, 2014). This strategy enhances the efficiency of the target protein in inducing immune responses against the tumor, which is important in advancing functional goals such as protein and effective drug delivery (Itani and Al Faraj, 2019; Trojer et al., 2013; Liu et al., 2014).

The unique coalescence of Cu NPs and Fe_3O_4 has found a broad range of utility in biological targeting, biological separation and high-density magnetic recording. So, we wish to report the synthesis, characterizations and applications of novel Cu NPs decorated PEG2000 modified-magnetite nanocomposite (Fe_3O_4/PEG_{2000}/Cu NPs) mediated by *Green Tea* extract as a reducing agent. The polyethylene glycol affords additional stability to the MNPs from unwanted oxidation and corrosion. Also, the modified surface can easily have capped the copper ions and stabilized the in *situ* reduced copper nanoparticles (Scheme 1). Also, the properties of Fe_3O_4/PEG_{2000}/Cu NPs against common gastric cancer cell lines i.e. NCI-N87 and MKN45 were evaluated.

2. Experimental

2.1. Preparation of ***Green Tea*** extract

0.2 gm of the dried *Green Tea* leaves were dispersed over 50 ml Milli-Q water and stirred vigorously at 80 °C for 20 min. Subsequently, the mixture was filtered over Whatman No. 1 paper to remove the undissolved plant residues. The colored filtrate was further centrifuged at 4000 rpm for 5 min and the clear supernatant layer was decanted off for further use.

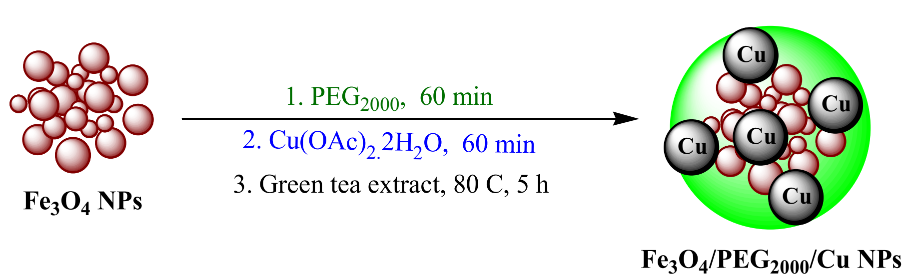

Scheme 1 Schematic preparation of Fe_3O_4/PEG_{2000}/Cu nanocomposite.

2.2. Synthesis of the $Fe_3O_4/PEG_{2000}/Cu$ nanocomposite

Fe_3O_4 NPs were prepared through the typical co-precipitation method as published earlier (Arunachalam et al., 2003). For preparing Fe_3O_4/PEG_{2000} nanocomposite, initially 0.5 g of the Fe_3O_4 NPs were uniformly dispersed in 100 ml water by sonication for 30 min and then a solution PEG_{2000} (0.2 g in 20 ml water) was added into it. The mixture was stirred for 2 h under ambient conditions for the possible surface modifications of Fe_3O_4 NPs. The as-synthesized Fe_3O_4/PEG_{2000} nanocomposite was retrieved magnetically and washed thoroughly with deionized water and re-dispersed in 50 ml water for the next step. Then, 0.1 g $Cu(OAc)_2{\cdot}2H_2O$ was dissolved in water and added to the above mixture and stirred for 60 min. Next, 20 ml aqueous *Green Tea* extract is added and stirred at 80 °C for 5 h. Next, the prepared $Fe_3O_4/PEG_{2000}/Cu$ nanocomposite was isolated by magnetic decantation, rinsed with DI-H_2O and treated in a vacuum at 40 °C. Finally, ICP-AES analysis was performed to assess the Cu content, as being 0.14 mmol/g.

2.3. Antioxidant activities of $Fe_3O_4/PEG_{2000}/Cu$ nanocomposite

This experiment was performed with few changes in the method of Lu et al (Lu et al., 2021). 0.5 ml of 0.1 mM DPPH solution prepared in 95% ethanol was mixed with 100 µl of $Fe_3O_4/PEG_{2000}/Cu$ nanocomposite. The resulting solution was kept in the dark at 38 °C for 31 min. The absorbance of the samples was then read at 518 nm. To compare the activity of $Fe_3O_4/PEG_{2000}/Cu$ nanocomposite; standard BHT compound was used as a standard antioxidant.

To determine the amount of IC50 (IC50 is defined as the concentration required to inhibit 50% of the antioxidant activity) for $Fe_3O_4/PEG_{2000}/Cu$ nanocomposite, experiments were performed at eleven different concentrations of the desired nanoparticle solution and BHT. Each experiment was performed in three shifts and the mean values were calculated. Percentage of radicalization activity was calculated through the following equation (Lu et al., 2021):

$$\text{Inhibition}\ (\%) = \frac{\text{Sample A.}}{\text{Control A.}} \times 100$$

In this regard, the blank adsorption indicates the adsorption of the control solution, which contains 0.5 ml of DMPH solution and 100 µl of 95% ethanol instead of $Fe_3O_4/PEG_{2000}/$ Cu nanocomposite solution and adsorption of the reaction indicates the adsorption of the solution content of the $Fe_3O_4/PEG_{2000}/Cu$ nanocomposite sample (Lu et al., 2021).

2.4. Anti-human gastric cancer properties of $Fe_3O_4/PEG_{2000}/Cu$ nanocomposite

NCI-N87 and MKN45 cells were used to evaluate the anticancer effect of $Fe_3O_4/PEG_{2000}/Cu$ nanocomposite on cell culture.

Because nanoparticles is not soluble directly in 1640-RPMI medium and also the solvent of dimethyl sulfoxide nanoparticles (DMSO) itself has cytotoxic effects, to eliminate the effect of this substance on treated cells, its amount in the final solution is considered less than 1%. Dimethyl sulfoxide is not toxic to concentrations less than 1% and the concentration of this solvent is important in this regard. For this purpose, 1000 µg of nanoparticle was dissolved in 100 µl of dimethyl sulfoxide solvent after weighing. Then 1 ml of culture medium was added for better dissolution and finally the volume of solution was increased to 24 ml using culture medium: Then, successive dilutions of this stock were used in the proportions of 1–1000 µg/ml. Eleven concentrations were used for the cell lines (Lu et al., 2021).

In this study, 100 µl of culture medium containing 10^4 cells per plate 96 were placed. After 24 h, incubation of concentrations of 1–1000 micrograms per milliliter of nanoparticles was added to the cells, and incubated for 24, 48, and 72 h, respectively. After these times, 20 µl of MTT plate with a concentration of 5 mg/ml was added to each cell and incubated in the dark for another 4 h. After some time, the MTT medium was carefully removed, and 200 µl of acidified isopropanol were added to each plate to remove the purple formanes. After 15 min of incubation at room temperature, the light absorption of each well was read using an ELISA at 570 nm against a reference wavelength of 690 nm. The findings were reported as cell survival and IC50 (concentration that inhibits cell growth up to 50%) based on the concentration curve (µg/ml) (Lu et al., 2021).

It should be noted that the effect of each concentration of the nanoparticles on cell lines was investigated in five independent experiments. According to the values of light absorption obtained by the ELISA reader, the percentage of growth inhibition related to each concentration was calculated using the following formula:

$$\text{Cell viability}\ (\%) = \frac{\text{Sample A.}}{\textit{Control A.}} \times 100$$

Finally, linear regression was done to gain IC50, which indicates the nanoparticles concentration, which causes 50% cancer cell growth inhibition. Using the curve, the line equation for cancer cells was obtained, respectively, then by replacing 50% inhibition in the equation, the IC50 value for cancer cells was obtained (Lu et al., 2021).

2.5. Statistical analysis

SPSS statistical software version 22 was used for data analysis and the findings were determined as the mean standard deviation of 5 replications. Data were analyzed using one-way analysis of variance and Duncan post hoc test and the significance level in the test was considered 0.05.

3. Results and discussion

Cancer is a genetic disease that includes 277 types of diseases. There are also more than 100,000 types of chemicals in our environment, of which only 35,000 have been analyzed and about 300 of them produce cancer. The remaining 65,000 chemicals in nature have not yet been tested. Cancer occurs due to uncontrolled cell division, which is the result of environmental factors and genetic disorders (Gao et al., 2015; Mohammed et al., 2016; Li and Gu, 2014; Yang et al., 2011; Xinli, 2012; Allen, 2002; Byrne et al., 2008). The four key genes involved in cancer cell conduction include DNA repair genes, tumor suppressor genes, oncogenes, and programmed death genes (Xinli, 2012; Allen, 2002; Byrne et al., 2008; Torchilin,

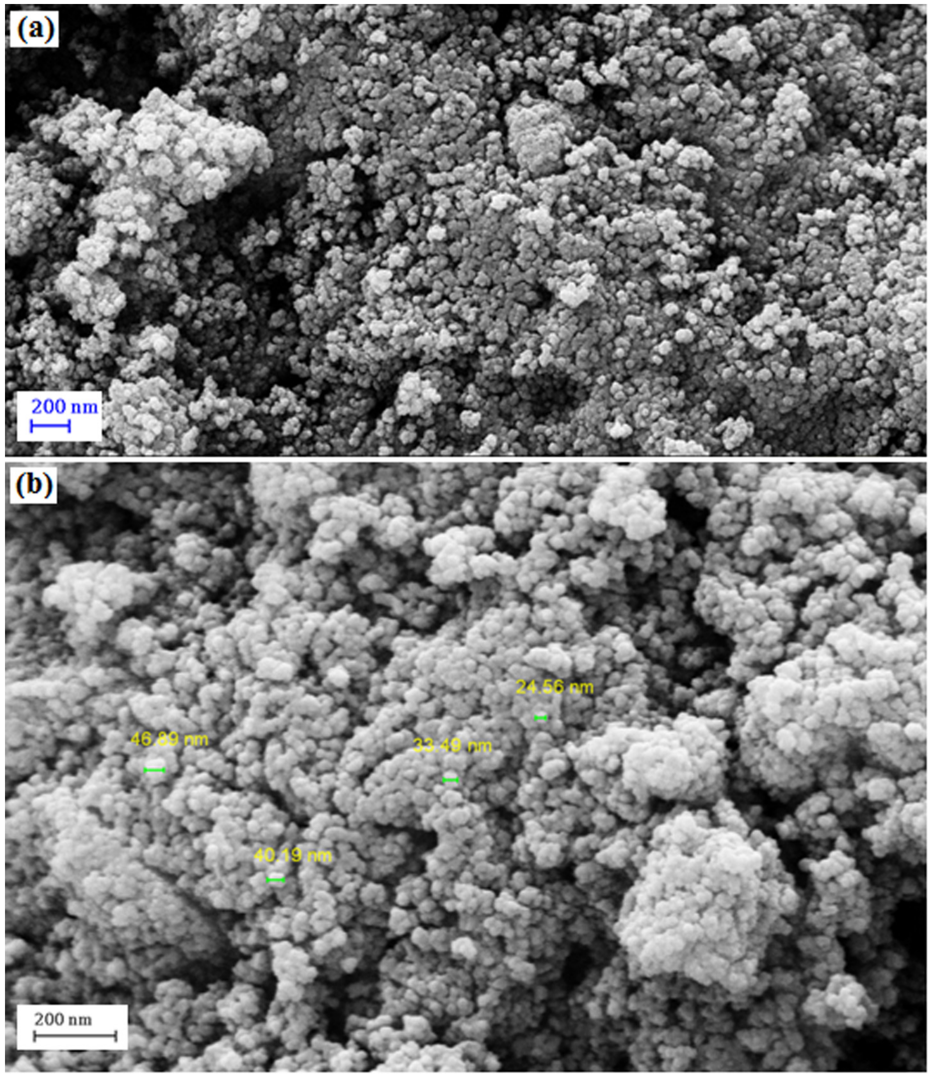

Fig. 1 FE-SEM images of (a) Fe_3O_4 and (b) $Fe_3O_4/PEG_{2000}/Cu$ nanocomposite.

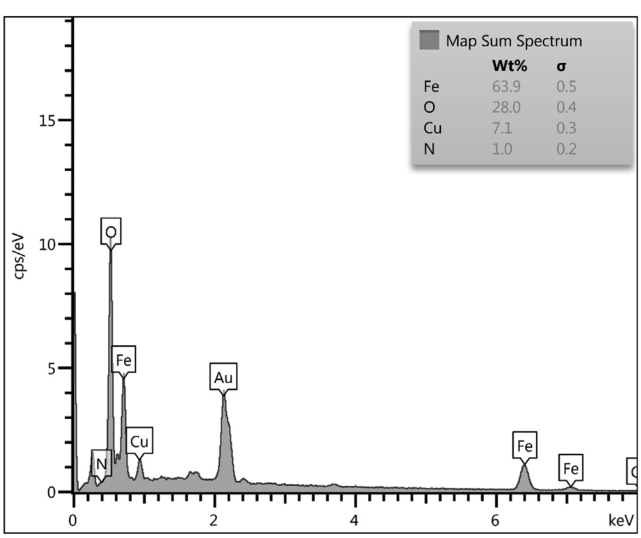

Fig. 2 EDX spectrum of the $Fe_3O_4/PEG_{2000}/Cu$ nanocomposite.

2007; Pranali, 2013). If a genetic mutation is produced in a cell, normal cells go out of their way and are affected by new commands that progress to cancer cells. In addition to chemicals, sunlight, shortwave, viruses and bacteria also have a special role in causing cancer (Byrne et al., 2008; Torchilin, 2007; Pranali, 2013; Zhang et al., 2014; Matsumura et al., Cancer 2004). Cancers have existed since the beginning of mankind. In recent decades, advances in computer molecular medicine have been able to not only study the causes and mechanisms of this deadly disease but also to perform better in its early diagnosis and treatment (Xinli, 2012; Allen, 2002; Byrne et al., 2008). More than 50% of cancers are currently being treated, especially if diagnosed early. Cancer can be treated in several ways: surgery, chemotherapy, radiation therapy, immunotherapy, gene therapy, or a combination of these. Due to the relative inefficiency and very severe side effects of chemotherapy drugs, researchers and scientists have sought a new formulation of various compounds, especially metallic nanoparticles (Matsumura et al., Cancer 2004,; Nie et al., 2007; Gao et al., 2002; Davis et al., 2008).

In the recent study, post-synthetic modification pathway was followed to prepare Fe_3O_4/PEG_{2000}/Cu nanocomposite (Scheme 1). First the magnetic Fe_3O_4 nanoparticles were coated by polyethylene glycol and next, the phytochemicals derived from the *Green Tea* extract acted as mild and benign reductant for the anchored Cu (II) ions Fe_3O_4/PEG_{2000} Matrix. The Fe_3O_4/PEG_{2000}/Cu nanocomposite was physicochemically characterized through FESEM, TEM, EDX, elemental mapping, VSM, XRD and ICP-AES analysis.

The detailed morphological structure, shape and size of the Fe_3O_4 and Fe_3O_4/PEG_{2000}/Cu nanocomposite was ascertained by SEM and TEM studies. The globular shape nanoparticles can be observed from SEM image having a mean diameter of the nanometer (Fig. 1). In addition, a continuous PEG biopolymer layer is seen on the Fe_3O_4 surface indicating the surface modification (Fig. 1b). There occurs a homogeneous growth of PEG over it. The agglomeration of nanocomposite particles can be understood due to manual sample preparation. The particles are almost homo-morphic and are sized between 20 and 40 nm.

EDX analysis of the Fe_3O_4/PEG_{2000}/Cu nanocomposite was executed to have sheer knowledge of constituent elements and it displays the occurrence of C, O, Fe and Cu elements (Fig. 2). The inset of the EDX profile clearly says that Cu content is 7.1%. This is probably due to excess deposition of Cu precursor. The non-metals justify the organochemical attachment and a successful surface modification of the Fe_3O_4 NP. The data obtained from EDX analysis were further rationalized through elemental mapping. X-ray scanning of a section of FESEM image reveals the uniform distribution of Fe, O, C and Cu atoms over the nanocomposite surface (Fig. 3).

The inherent structural features are demonstrated via TEM study of the nanocomposite. The Fe_3O_4/PEG_{2000} and Fe_3O_4/PEG_{2000}/Cu nanocomposite TEM analysis (Fig. 4) displayed the decoration of the Cu NPs with spherical morphology and dark spots on the magnetic PEG surface. The tiny black dots correspond to the Cu NPs, being of ~20–30 nm in size. The PEG polymer conjugate favors Cu NPs by electrostastic force of attraction and thereby gets stabilized. These data clearly demonstrate the proposed architecture of the material.

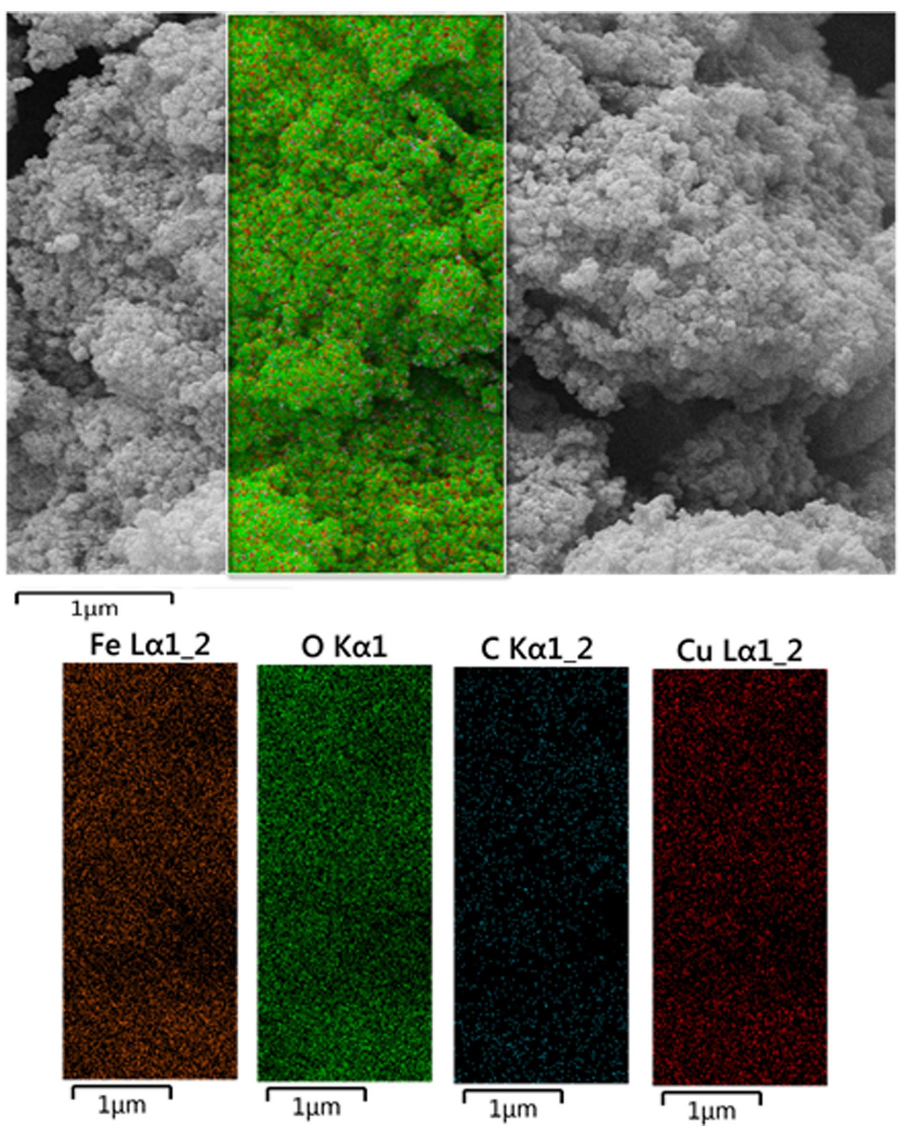

Fig. 3 FE-SEM image of Fe_3O_4/PEG_{2000}/Cu nanocomposite with its elemental mapping.

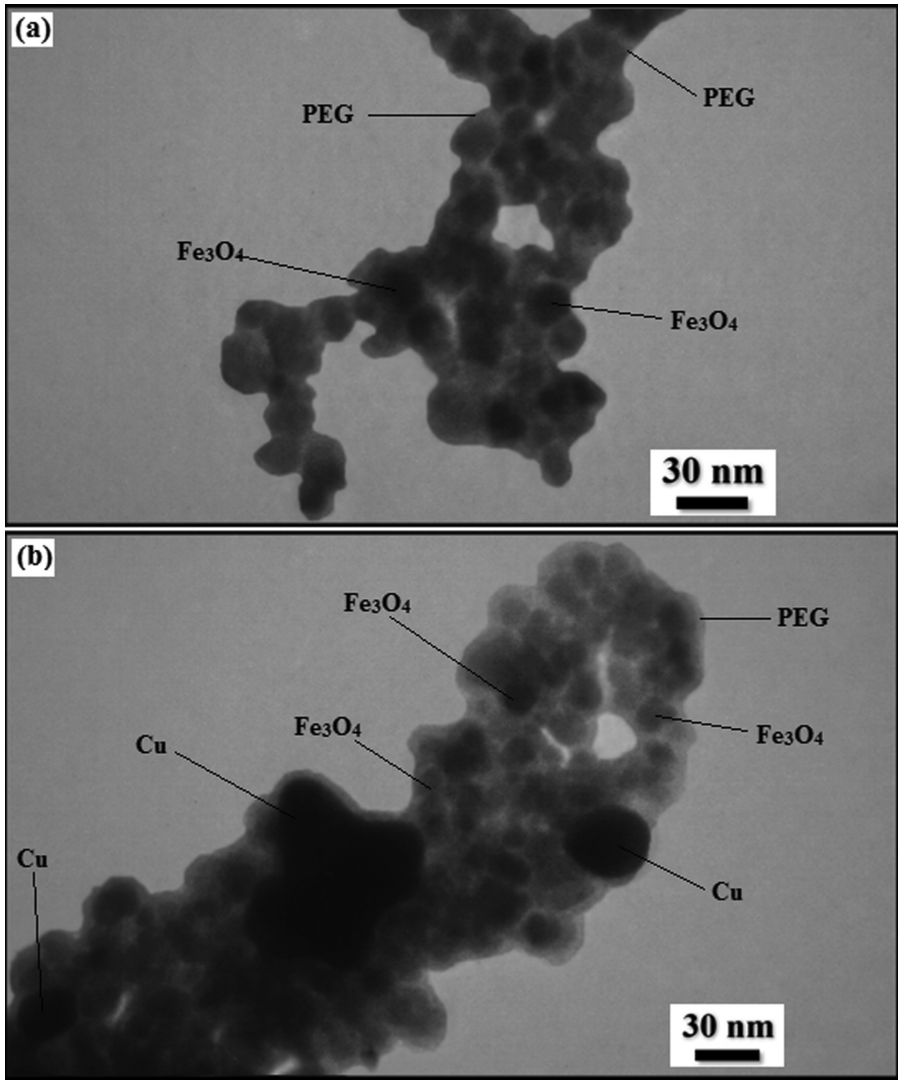

Fig. 4 TEM images of (a) Fe_3O_4/PEG_{2000} and (b) Fe_3O_4/PEG_{2000}/Cu nanocomposite.

The presence of Cu and Fe_3O_4 was verified with XRD analysis. Fig. 5 exhibits the crystalline phases of Fe_3O_4/PEG_{2000}/Cu nanocomposite being determined over XRD. The said profile demonstrates the typical peaks of cubic spinel Fe_3O_4 NPs. The characteristic peaks observed at 2θ = 30.1, 35.4, 43.3, 53.6, 57.2 and 62.8 closely resembles to ferrite NPs that are corroborated to the (220), (311), (400), (422), (511) and (440) diffraction planes (JCPDS No. 19-0629). This suggests that the inner core structure remained undisturbed even after modification with PEG and copper. The extra peaks appeared at 2θ = 43.1, 49.6 and 75.4 can be allocated to the (111), (200) and (220) planes of Cu *fcc* crystalline phases.

The saturation magnetization (*M*s) value obtained from magnetic hysteresis loops of Fe_3O_4/PEG_{2000}/Cu nanocomposite was 27.8 emu/g (Fig. 6).

Oxidative stress is caused by an imbalance between the production of free radicals and metabolic reactions, which leads to damage to lipids, proteins and nucleic acids. These damages may be due to low levels of antioxidants or an excessive increase in the production of free radicals in the body (Namvar et al., 2014; Sankar et al., 2014; Katata-Seru et al., 2018). In humans, oxidative stress is associated with chronic diseases such as diabetes and cancer. Therefore, the production of synthetic and natural antioxidants is necessary to prevent oxidative stress and its destructive effects. Antioxidants effectively and in various ways reduce the harmful effects of free radicals in the biological and food systems and cause detoxification (Sankar et al., 2014; Katata-Seru et al., 2018; Sangami and Manu, 2017). In this regard, green nanoparticles can be used (using plant substrates to prepare nanomaterials that are environmentally friendly and do not contain any harmful chemicals) that show antioxidant properties. At present, the use of non-toxic substances in synthesizing nanoparticles to prevent biological hazards, especially in medical and pharmaceutical applications is considered (Namvar et al., 2014; Sankar et al., 2014; Katata-Seru et al., 2018; Sangami and Manu, 2017; Beheshtkhoo et al., 2018; Radini et al., 2018). Many researchers have focused on bioactive substances derived from plants or other sources such as bacteria, fungi and yeast for synthesizing nanoparticles. The green synthesis

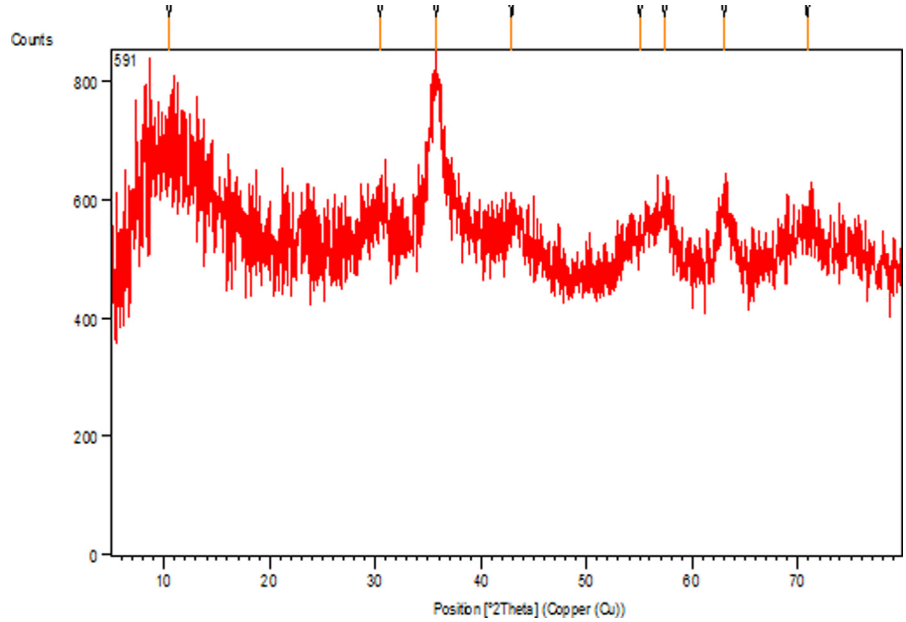

Fig. 5 X-ray diffraction study of Fe_3O_4/PEG_{2000}/Cu nanocomposite.

method is thought to increase the biocompatibility and performance of metal nanoparticles for biological applications due to removing harmful chemicals (Davis et al., 2008; Namvar et al., 2014; Sankar et al., 2014; Katata-Seru et al., 2018). During the bioproduction stages of nanoparticles, their extracellular production using plants or their extracts is more beneficial and their production can be adjusted in a controlled way based on size, distribution and shape for different purposes (Davis et al., 2008; Namvar et al., 2014; Sankar et al., 2014; Katata-Seru et al., 2018; Sangami and Manu, 2017; Beheshtkhoo et al., 2018).

In the recent study, the scavenging capacity of Fe_3O_4/PEG_{2000}/Cu nanocomposite and BHT at different concentrations expressed as percentage inhibition has been indicated in Tables 1 and Fig. 7. In the antioxidant test, the IC50 of Fe_3O_4/PEG_{2000}/Cu nanocomposite and BHT against DPPH free radicals were 198 and 85 µg/mL, respectively (Tables 1).

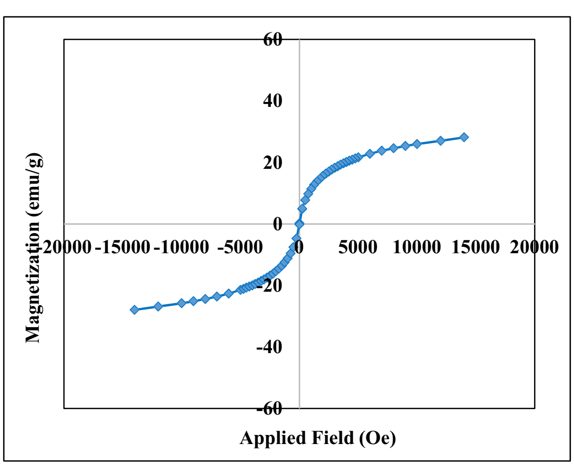

Fig. 6 Hysteresis loops of Fe_3O_4/PEG_{2000}/Cu nanocomposite.

Table 1 The IC50 of Fe_3O_4/PEG_{2000}/Cu nanocomposite and BHT in the antioxidant test.

	Fe_3O_4/PEG_{2000}/Cu nanocomposite	BHT
IC50 (µg/mL)	198 ± 0^b	85 ± 0^a

The numbers indicate the percent of free radical (DPPH) inhibition at the concentrations of 0–1000 µg/mL of Fe_3O_4/PEG_{2000}/Cu nanocomposite (I) and BHT (II).

In recent decades, the power of nanotechnology has been used in countless fields, including biomedical sciences. Nanoparticles are solid colloidal particles with dimensions of 1 to 100 nm (Cardoso et al., 2018; Khanna et al., 2018; Xie et al., 2018). Due to their comparable dimensions to cells, viruses, proteins, and genes, they can interact with basic biological processes. In recent years, much attention has been paid to synthesizing different types of nanoparticles as nanomedical materials. Among them, magnetic nanoparticles made of iron, cobalt or nickel oxides have special properties such as high surface-to-volume ratio and high magnetic properties, allowing for potential manipulation by an external magnetic field (Wei et al., 2008; Pascal et al., 1999; Bomatí-Miguel et al., 2008). In particular, magnetic nanoparticles produced with ferromagnetic material, iron oxide nanoparticles (IONPs), made of magnetite (Fe_3O_4) and magnitude (Fe03-) have wide applications in medicine such as targeted drug delivery, hyperthermia, photography and biosensors (Xie et al., 2018; Wei et al., 2008; Pascal et al., 1999; Bomatí-Miguel et al., 2008). In recent decades, much research has been done on synthesizing iron oxide nanoparticles and many reports have described efficient synthesis approaches for the production of controlled, stable, biocompatible, and integrated iron oxide nanoparticles (Khanna et al., 2018; Xie et al., 2018; Wei et al., 2008;

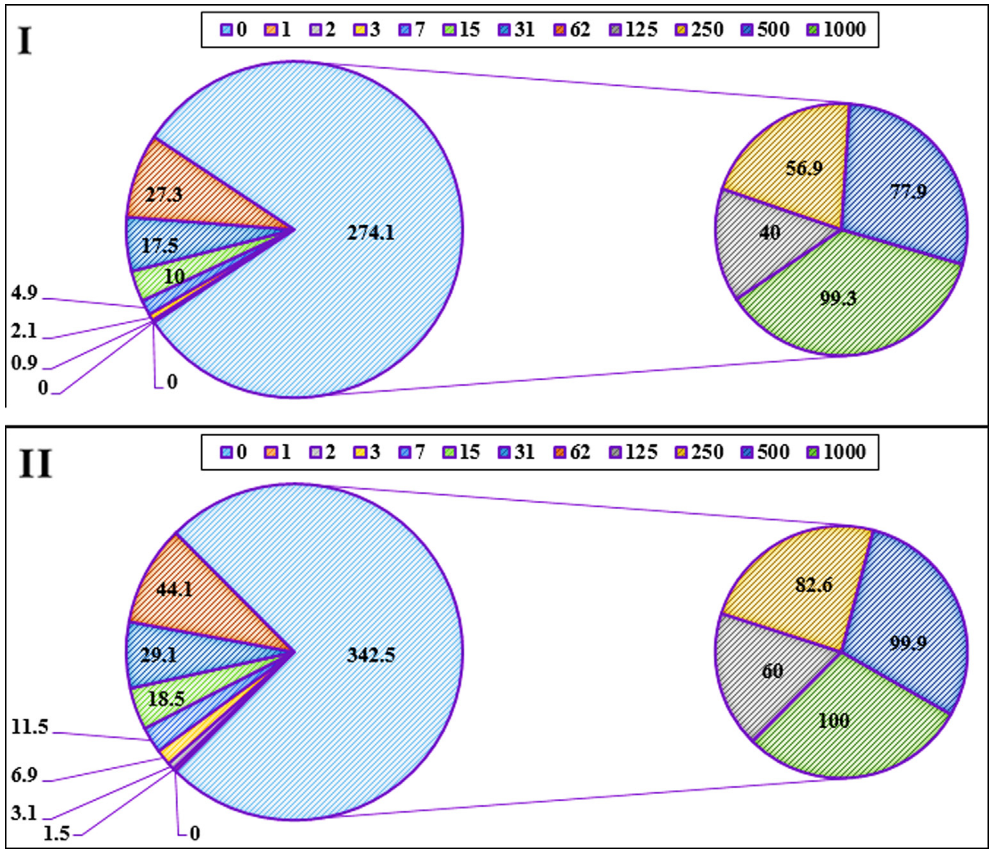

Fig. 7 The antioxidant properties of Fe_3O_4/PEG_{2000}/Cu nanocomposite (I) and BHT (II) against DPPH.

Pascal et al., 1999). The most common methods such as co-precipitation, hydrothermal synthesis, microemulsion, sonochemical synthesis can lead to the high-quality synthesis of iron oxide nanoparticles. In addition, these nanoparticles can be prepared by other methods such as electrochemical synthesis, laser pyrolysis technique, synthesis with microorganisms or bacteria (especially magneto-tactical bacteria and iron-reducing bacteria) (Wei et al., 2008; Pascal et al., 1999; Bomatí-Miguel et al., 2008; Bharde et al., 2008; Roh et al., 2006; Faraji et al., 2010). Low toxicity and high biocompatibility of magnetite nanoparticles have led to the expansion of magnetite nanoparticles in targeted drug delivery. Using an external magnetic field, the nanoparticles can be directed to the target tissue and release the drug at the target site (Bharde et al., 2008; Roh et al., 2006; Faraji et al., 2010; Mou et al., 2015; Renard, 2009). Targeted drug delivery reduces the side effects of the drug to surrounding healthy tissues and also reduces the dose of drug required. To increase the biocompatibility of magnetite nanoparticles for use in the field of drug delivery, magnetite nanoparticles are modified by organic or inorganic coatings (Bharde et al., 2008; Roh et al., 2006; Faraji et al., 2010; Mou et al., 2015). Coating magnetite nanoparticles with the right combination can control the loading, delivery and release of the drug. In addition, suitable coatings can reduce the toxicity of nanoparticles and increase their biocompatibility (Pascal et al., 1999; Bomatí-Miguel et al., 2008; Bharde et al., 2008). Many cancer drugs are loaded onto magnetic drug carriers through various interactions. Coating magnetite nanoparticles with polymers is an ideal method of drug delivery; because in addition to reducing carrier toxicity, it also prevents magnetite nanoparticles from clotting (Renard, 2009; Schroeder et al., 2012; Gobbo et al., 2015).

Another application of magnetite nanoparticles is the use of thermotherapy. Due to the high sensitivity of cancer cells to temperatures above 42°, it disrupts the natural enzymatic processes that keep cells alive, and ultimately leads to the death of cancer cells (Schroeder et al., 2012; Gobbo et al., 2015; Will et al., 2006). In this method, non-ionizing electromagnetic waves increase the temperature in the tumor tissue. Because cancer cells are more sensitive to temperature rise than healthy cells, selective destruction of cancer cells occurs (Mou et al., 2015; Renard, 2009; Schroeder et al., 2012; Gobbo et al., 2015; Will et al., 2006). Treatment of the metastatic disease depends on diagnostic tools that can pinpoint the exact location of the metastatic cancer cells. Imaging technology currently in use is inaccurate in finding cancer cells hidden in other organs (Schroeder et al., 2012; Gobbo et al., 2015; Will et al., 2006; Harada et al., 2007). Therefore, magnetic iron oxide nanoparticles can be used for cell imaging. Magnetic iron nanoparticles as an imaging agent are a powerful tool for detecting metastases (Will et al., 2006; Harada et al., 2007). Iron oxide nanoparticles can be modified with specific molecules or antigens present on the surface of the metastatic cancer cells and enable the detection of target cells using MRI. The detection of lymph node metastases using iron oxide nanoparticles has been investigated in recent years, which shows promising results (Schroeder et al., 2012; Gobbo et al., 2015; Will et al., 2006; Harada et al., 2007).

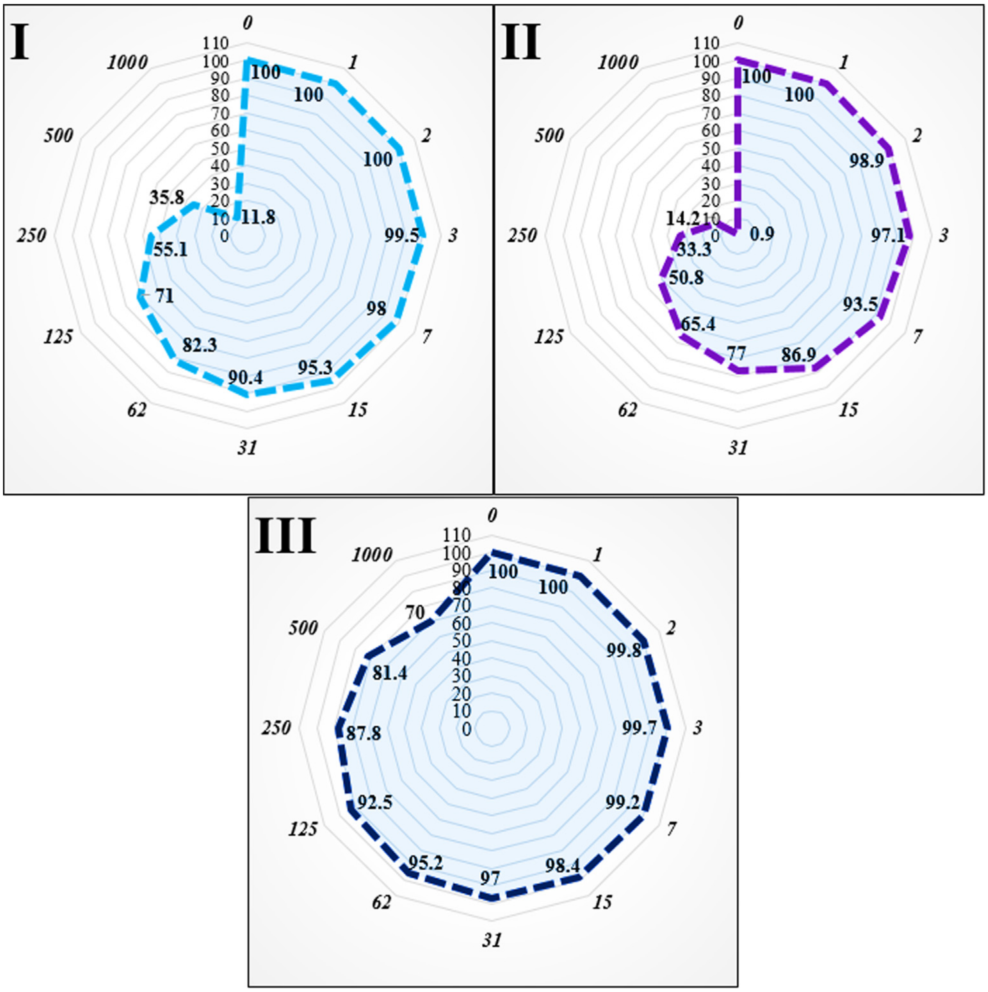

Fig. 8 The anti-human gastric cancer properties (Cell viability (%)) of $Fe_3O_4/PEG_{2000}/Cu$ nanocomposite (Concentrations of 0–1000 μg/mL) against human gastric cancer (NCI-N87 (I) and MKN45 (II)) and normal (HUVEC: III) cell lines.

In this investigation, the treated cells with different concentrations of the present $Fe_3O_4/PEG_{2000}/Cu$ nanocomposite were assessed by MTT assay for 48 h about the cytotoxicity properties on normal (HUVEC) and gastric malignancy cell lines i.e. NCI-N87 and MKN45 (Fig. 8).

The viability of malignant gastric cell line reduced dose-dependently in the presence of $Fe_3O_4/PEG_{2000}/Cu$ nanocomposite. The IC50 of $Fe_3O_4/PEG_{2000}/Cu$ nanocomposite were 316 and 131 μg/mL against NCI-N87 and MKN45 cell lines, respectively (Table 2).

The absorbance rate was evaluated at 570 nm, which represented viability on normal cell line (HUVEC) even up to 1000 μg/mL for $Fe_3O_4/PEG_{2000}/Cu$ nanocomposite (Table 2 and Fig. 8).

Table 2 The IC50 of $Fe_3O_4/PEG_{2000}/Cu$ nanocomposite in the anti-human gastric cancer test.

	NCI-N87	MKN45	HUVEC
IC50 (μg/mL)	316 ± 0^{b}	131 ± 0^{a}	–

The numbers indicate the percent of cell viability at the concentrations of 0–1000 μg/mL of $Fe_3O_4/PEG_{2000}/Cu$ nanocomposite against several human gastric cancer cell lines.

4. Conclusion

This study demonstrates an effective, simple, green and cost-effective method for preparing $Fe_3O_4/PEG_{2000}/Cu$ nanocomposite applying *Green Tea* extract as a green reductant and using PEG as stabilizer agent of the Cu NPs. The particles were characterized by FE-SEM, EDS, TEM, XRD, ICP and VSM techniques.

The viability of malignant gastric cell line reduced dose-dependently in the presence of $Fe_3O_4/PEG_{2000}/Cu$ nanocomposite. The IC50 of $Fe_3O_4/PEG_{2000}/Cu$ nanocomposite were 316 and 131 μg/mL against NCI-N87 and MKN45 cell lines, respectively. The $Fe_3O_4/PEG_{2000}/Cu$ nanocomposite showed the best antioxidant activities against DPPH. The IC50 of $Fe_3O_4/PEG_{2000}/Cu$ nanocomposite and BHT against DPPH free radicals were 198 and 85 μg/mL, respectively. After clinical study, $Fe_3O_4/PEG_{2000}/Cu$ nanocomposite can be utilized as an efficient drug in the treatment of gastric cancer in humans.

Declaration of Competing Interest

The authors declare that they have no known competing financial interests or personal relationships that could have appeared to influence the work reported in this paper.

References

Allen, T.M., 2002. Ligand-targeted therapeutics in anticancer therapy. Nat. Rev. Cancer 2 (10), 750–763.

Arunachalam, K.D. et al, 2003. One-step green synthesis and characterization of leaf extract-mediated biocompatible silver and gold nanoparticles from Memecylon umbellatum. Int. J. Nanomed. 8, 1307–1315.

Bao, G., Mitragotri, S., Tong, S., 2013. Multifunctional nanoparticles for drug delivery and molecular imaging. Ann. Rev. Biomedl. Engin. 15, (1) 253282.

Bastus, N.G., Sanchez-Tillo, E., Pujals, S., et al, 2009. Peptides conjugated to gold nanoparticles induce macrophage activation. Mol. Immunol. 46 (743), 748.

Beheshtkhoo, N., Kouhbanani, M.A.J., Savardashtaki, A., et al, 2018. Green synthesis of iron oxide nanoparticles by aqueous leaf extract of Daphne mezereum as a novel dye removing material. Appl. Phys. A 124, 363–369.

Bharde, A.A., Parikh, R.Y., Baidakova, M., Jouen, S., Hannoyer, B., Enoki, T., et al, 2008. Bacteria-mediated Precursor-Dependent Biosynthesis of Superparamagnetic Iron Oxide and Iron Sulfide Nanoparticles. Langmuir 24, 5787.

Bomatí-Miguel, O., Mazeina, L., Navrotsky, A., Veintemillas-Verdaguer, S., 2008. Calorimetric Study of Maghemite Nanoparticles Synthesized by LaserInduced Pyrolysis. Chem. Mater. 20, 591.

Borm, P.J., Robbins, D., Haubold, S., et al, 2006. The potential risks of nanomaterials: a review carried out for ECETOC. Particle Fibre Toxicol. 3 (1), 11.

Byrne, J.D., Betancourt, T., Brannon-Peppas, L., 2008. Active targeting schemes for nanoparticle systems in cancer therapeutics. Adv. Drug Del. Rev. 60 (15), 1615–1626.

Cardoso, V.F., Francesko, A., Ribeiro, C., Bañobre-López, M., Martins, P., Lanceros-Mendez, S., 2018. Advances in Magnetic Nanoparticles for Biomedical Applications. Adv. Healthc. Mater.

(a) Celardo, I., Pedersen, J.Z., Traversa, E., Ghibelli, L., 2011. Nanoscale 3(4), 1411-1420; (b) Kiani, A., Nabiyouni, G., Masoumi, S., Ghanbari, D., 2019. Composites Part B: Eng. 175, 107080; (c) Joulaei, M., Hedayati, K., Ghanbari, D., 2019. Composites Part B: Eng. 176, 107345; (d) Ahmadian-Fard-Fini, Ghanbari, D., Amiri, O., Salavati-Niasari, M., 2020. Carbohydrate polymers 229, 115428; (e) Moradi, B., Nabiyouni, G., Ghanbari, D., 2018. J. Mater. Sci.: Mater. Electron. 29, 11065-11080; (f) Masoumi, S., Nabiyouni, G., Ghanbari, D., 2016. J. Mater. Sci.: Mater. Electron. 27, 11017-11033; (g) Esmaeili-Bafghi-Karimabad, A., Ghanbari, D., Salavati-Niasari, M., Nejati-Moghadam, L., Gholamrezaei, S., 2015. J. Mater. Sci.: Mater. Electron. 26, 6970-6978; (h) Gholamian, F., Salavati-Niasari, M., Ghanbari, D., Sabet, M., 2013. J. Cluster Sci. 24, 73-84; (j) Veisi, H., Sedrpoushan, A., Faraji, A.R., Heydari, M., Hemmati, S., Fatahi, B., 2015. RSC Adv. 5, 68523-68530; (k) Veisi, H., Safarimehr, P., Hemmati, S., 2019. Mater. Sci. Eng.: C 96, 310-318; (l) Veisi, H., Mohammadi, L., Hemmati, S., Tamoradi, T., Mohammadi, P., 2019. ACS Omega 4, 13991-1400; (m) Veisi, H., Manesh, A.A., Eivazi, N., Faraji, A.R., 2015. RSC Adv. 5, 20098-20107; (n) Maleki, B., Hemmati, S., Sedrpoushan, A., Ashrafi, S.S., Veisi, H., 2014. RSC Adv. 4, 40505-40510; (o) Hemmati, S., Mehrazin, L., Pirhayati, M., Veisi, H., 2019. Polyhedron 158, 414-422; (p) Baghayeri, M., Amiri, A., Alizadeh, Z., Veisi, H., Hasheminejad, E., 2018. J. Electroanaly. Chem. 810, 69-77.

Davis, M.E., Chen, Z., Shin, D.M., 2008. Nanoparticle therapeutics: an emerging treatment modality for cancer. Nat Rev Drug Discov. 7 (9), 771–782.

De Jong, W.H., Borm, P.J., 2008. Drug delivery and nanoparticles: applications and hazards. Int. J. Nanomed. 3 (2), 133–149.

Faraji, M., Yamini, Y., Rezaee, M., 2010. Magnetic nanoparticles: Synthesis, stabilization, functionalization, characterization, and applications. J. Iran. Chem. Soc. 7 (1), 1–37.

Gao, Z., Lukyanov, A.N., Singhal, A., Torchilin, V.P., 2002. Diacyl-lipid-polymer micelles as nanocarriers for poorly soluble anticancer drugs. Nano Lett. 2 (9), 979–982.

Gao, J., Wang, Z., Liu, H., Wang, L., Huang, G., 2015. Liposome encapsulated of temozolomide for the treatment of glioma tumor: preparation, characterization and evaluation. Drug Discov Ther. 9 (3), 205–212.

Gobbo, L., Sjaastad, K., Radomski, M.W., Volkov, Y., Prina-Mello, A., 2015. Magnetic nanoparticles in cancer theranostics. Theranostics 5 (11), 1249–1263.

Harada, T., Tanigawa, N., Matsuki, M., Nohara, T., Narabayashi, I., 2007. Evaluation of lymph node metastases of breast cancer using ultrasmall superparamagnetic iron oxide-enhanced magnetic resonance imaging. Eur. J. Radiol. 63 (3), 401–407.

Itani, R., Al Faraj, S.A., 2019. siRNA Conjugated Nanoparticles-A Next Generation Strategy to Treat Lung Cancer. Int. J. Mol. Sci. 20 (23), 6088.

Katata-Seru, L., Moremedi, T., Aremu, O.S., et al, 2018. Green synthesis of iron nanoparticles using Moringa oleifera extracts and their applications: Removal of nitrate from water and antibacterial activity against Escherichia coli. J. Mol. Liq. 256, 296–304.

Khanna, L., Verma, N.K., Tripathi, S.K., 2018. Burgeoning tool of biomedical applicationsSuperparamagnetic nanoparticles. J. Alloy. Compd. 752, 332–353.

Langer, R., 1990. New methods of drug delivery. Science 249, 1527–1533.

LaVan, D.A., McGuire, T., Langer, R., 2003. Smallscale systems for in vivo drug delivery. Nat. Biotechnol. 21, 1184–1191.

Li, Y.N., Gu, F., 2014. Recent progress in doxorubicin nano-drug delivery systems for reserving multidrug resistance 11(3), 177-181.

Liu, D., Chen, L., Jiang, S., et al, 2014. Formulation and characterization of hydrophilic drug diclofenac sodium-loaded solid lipid nanoparticles based on phospholipid complexes technology. J. Liposome Res. 24 (1), 17–26.

Lu, Y., Wan, X., Li, L., Sun, P., Liu, G., 2021. Synthesis of a reusable composite of graphene and silver nanoparticles for catalytic reduction of 4- nitrophenol and performance as anti-colorectal carcinoma. J. Mater. Res. Technol. 12, 1832–1843.

Mao, B.H. et al, 2016. Mechanisms of silver nanoparticle-induced toxicity and important role of autophagy. Nanotoxicol. 10, 1021–1040.

Matsumura, Y., Hamaguchi, T., Ura, T., Muro, K., Yamada, Y., Shimada, Y., Shirao, K., Okusaka, T., Ueno, H., Ikeda, M., et al, Cancer 2004,. Phase I clinical trial and pharmacokinetic evaluation of NK911, a micelleencapsulated doxorubicin. Br. J. Cancer 91, 1775–1781.

Mohammed, M.I., Makky, A.M., Teaima, M.H., Abdellatif, M.M., Hamzawy, M.A., Khalil, M.A., 2016. Transdermal delivery of vancomycin hydrochloride using combination of nano-ethosomes and iontophoresis: in vitro and in vivo study. Drug Deliv. 23 (5), 1558–1564.

Mou, X., Ali, Z., Li, S., He, N., 2015. Applications of magnetic nanoparticles in targeted drug delivery system. J. Nanosci. Nanotechnol. 15 (1), 54–629.

Namvar, F., Rahman, H.S., Mohamad, R., et al, 2014. Cytotoxic effect of magnetic iron oxide nanoparticles synthesized via seaweed aqueous extract. Int. J. Nanomed. 19, 2479–2488.

Nanosci, J., Roh, Y., Vali, H., Phelps, T.J., Moon, J.W., 2006. Extracellular Synthesis of Magnetite and MetalSubstituted Magnetite Nanoparticles. J. Nanosci. Nanotechnol. 6, 3517–3520.

Nie, S., Xing, Y., Kim, G.J., Simons, J.W., 2007. Nanotechnology applications in cancer. Annu. Rev. Biomed. Eng. 9, 257–288.

Pascal, C., Pascal, J.L., Favier, F., Moubtassim, M.L.E., Payen,, 1999. C Electrochemical Synthesis for the Control of y-Fe2O3 Nanoparticle Size. Morphology, Microstructure, and Magnetic Behavior. Chem. Mater. 11, 141.

Patra, J.K., Das, G., Fraceto, L.F., Campos, E.V.R., Rodriguez-Torres, M.D.P., Acosta-Torres, L.S., DiazTorres, L.A., Grillo, R., Swamy, M.K., Sharma, S., et al, 2018. Nano based drug delivery systems: Recent developments and future prospects. J. Nanobiotechnol. 16, 71.

Pranali, P., 2013. Deshpande, Current trends in the use of liposomes for tumor targeting. Nanomedicine 8 (9), 1509–1528.

Radini, I.A., Hasan, N., Malik, M.A., et al, 2018. Biosynthesis of iron nanoparticles using Trigonella foenum-graecum seed extract for photocatalytic methyl orange dye degradation and antibacterial applications. J. Photochem. Photobiol., B 183, 154–163.

Renard, P.E. et al, 2009. Local moderate magnetically induced hyperthermia using an implant formed in situ in a mouse tumor model. Int. J. Hyperth. 25 (3), 229–239.

Sangami, S., Manu, M., 2017. Synthesis of Green Iron Nanoparticles using Laterite and their application as a Fenton-like catalyst for the degradation of herbicide Ametryn in water. Environ. Technol. Innov. 8, 150–163.

Sankar, R., Maheswari, R., Karthik, S., et al, 2014. Anticancer activity of Ficus religiosa engineered copper oxide nanoparticles. Mat. Sci. Eng. C 44, 234–239.

Schroeder, A., Heller, D.A., Winslow, M.M., et al, 2012. Treating metastatic cancer with nanotechnology. Nat. Rev. Cancer 12 (1), 39–50.

Shi, J., Xiao, Z., Kamaly, N., Farokhzad, O.C., 2011. Selfassembled targeted nanoparticles: Evolution of technologies and bench to bedside translation. Acc. Chem. Res. 44, 1123–1134.

Stapleton, P.A., Nurkiewicz, T.R., 2014. Vascular distribution of nanomaterials. Wiley Interdisciplinary Reviews. Nanomed Nanobiotechnol. 6 (4), 338–348.

(a) Staroverov, S.A., Aksinenko, N.M., Gabalov, K.P., Vasilenko, O. A., Vidyasheva, I.V., Shchyogolev, S.Y.U., Dykman, L.A., 2009. Effect of gold nanoparticles on the respiratory activity of peritoneal macrophages. Gold Bull. 42 (2), 153-156; 21. (b) Karimi Ghezeli, Z., Hekmati, M., Veisi, H., 2019. Synthesis of Imatinib-loaded chitosan-modified magnetic nanoparticles as an anti-cancer agent for pH responsive targeted drug delivery. Appl. Organometallic Chem. 33, e4833; (c) Ghorbani-Vaghei, R., Hemmati, S., Hekmati, M., 2016. Pd immobilized on modified magnetic Fe_3O_4 nanoparticles: Magnetically recoverable and reusable Pd nanocatalyst for Suzuki-Miyaura coupling reactions and Ullmann-type N-arylation of indoles, J. Chem. Sci. 128, 1157-1162; (d) Wei Zhang, Hojat Veisi, Reyhaneh Sharifi, Delafarin Salamat, Bikash Karmakar, Malak Hekmati, Saba Hemmati, Mohammad Mahdi Zangeneh, Zhiyong Zhang, Qiang Su, 2020. Fabrication of Pd NPs on pectin-modified Fe_3O_4 NPs: A magnetically retrievable nanocatalyst for efficient C–C and C–N cross coupling reactions and an investigation of its cardiovascular protective effects, Int. J. Biol. Mac. 160, 1252-1262; (e) Entezari, M., Safari, M., Hekmati, M., Hekmat, S., Azin, A., 2014. Modification of carboxylated multiwall nanotubes with benzotriazole derivatives and study of their anticancer activities. Med. Chem. Res. 23, 487-495; (f) Azizian, J., Hekmati, M., Dadras, O.G., 2014. Functionalization of carboxylated multiwall nanotubes with dapsone derivatives and study of their antibacterial activities against E. coli and S. aureus. Orient. J. Chem. 30, 667-673; (g) Salehi, M.H., Yousefi, M., Hekmati, M., Balali, E., 2019. In situ biosynthesis of palladium nanoparticles on Artemisia abrotanum extract-modified graphene oxide and its catalytic activity for Suzuki coupling reactions, Polyhedron 165, 132-137; (h) Veisi, H., Karmakar, B., Tamoradi, T., Hemmati, S., Hekmati, M., Hamelian, M., 2021. Biosynthesis of CuO nanoparticles using aqueous extract of herbal tea (*Stachys Lavandulifolia*) flowers and evaluation of its catalytic activity, Sci. Rep. 11, 1983.

Torchilin, V.P., 2007. Targeted pharmaceutical nanocarriers for cancer therapy and imaging. AAPS J. 9, E128–E147.

Trojer, M.A., Li, Y., Wallin, M., Holmberg, K., Nyden, M., 2013. Charged microcapsules for controlled release of hydrophobic actives Part II: surface modification by Lbl adsorption and lipid bilayer formation on properly anchored dispersant layers. J. Colloid Interface Sci. 409, 8–17.

Wei, Wu, Quanguo, He, Changzhong, Jiang, 2008. Magnetic Iron Oxide Nanoparticles: Synthesis and Surface Functionalization Strategies. Nanoscale Res. Lett. 3 (11), 397–415.

Will, Purkayastha, S., Chan, C., et al, 2006. Diagnostic precision of nanoparticle-enhanced MRI for lymph-node metastases: a meta-analysis. Lancet Oncol. 7 (1), 52–60.

Xie, W., Guo, Z., Gao, F., Gao, Q., Wang, D., Liaw, B.S., Cai, Q., Sun, X., Wang, X., Zhao, L., 2018. Shape-, size- and structure-controlled synthesis and biocompatibility of iron oxide nanoparticles for magnetic theranostics. Theranostics. 8, 32843307.

Xinli, D.H.Z.S., 2012. Applications of nanocarriers with tumor molecular targeted in chemotherapy. Chemistry 75 (7), 621–627.

Yang, F., Jin, C., Jiang, Y., et al, 2011. Liposome based delivery systems in pancreatic cancer treatment: from bench to bedside. Cancer Treat. Rev. 37 (8), 633–642.

You, C., Han, C., Wang, X., et al, 2012. The progress of silver nanoparticles in the antibacterial mechanism, clinical application and cytotoxicity. Mol. Biol. Rep. 39, 9193–9201. https://doi.org/10.1007/s11033-012-1792-8.

Zhang, Y., Huang, Y., Li, S., 2014. Polymeric micelles: Nanocarriers for cancer-targeted drug delivery. AAPS PharmSciTech 15, 862–871.